Multiple mechanisms regulate NuMA dynamics at spindle poles

Olga Kisurina-Evgenieva[1,*], Gary Mack[2,‡], Quansheng Du[3], Ian Macara[3], Alexey Khodjakov[1] and Duane A. Compton[2,§]

[1]Division of Molecular Medicine, Wadsworth Center, New York State Department of Health, Albany, NY 12201, USA
[2]Department of Biochemistry, Dartmouth Medical School, Hanover, NH 03755, USA
[3]Center for Cell Signaling, Box 800977, HSC, University of Virginia, Charlottesville, VA 22908, USA
*Present address: Department of Cytology and Histology, Moscow State University, Moscow 119899, Russia
‡Present address: Cytoskeleton Incorporated, Denver, CO 80206, USA
§Author for correspondence (e-mail: duane.a.compton@dartmouth.edu)

Accepted 29 September 2004
Journal of Cell Science 117, 6391-6400 Published by The Company of Biologists 2004
doi:10.1242/jcs.01568

Summary

The large coiled-coil protein NuMA plays an essential role in organizing microtubule minus ends at spindle poles in vertebrate cells. Here, we use both in vivo and in vitro methods to examine NuMA dynamics at mitotic spindle poles. Using fluorescence recovery after photobleaching, we show that an exogenously expressed green-fluorescent-protein/NuMA fusion undergoes continuous exchange between soluble and spindle-associated pools in living cells. These dynamics require cellular energy and display an average half-time for fluorescence recovery of ~3 minutes. To explore how NuMA dynamics at spindle poles is regulated, we exploited the association of NuMA with microtubule asters formed in mammalian mitotic extracts. Using a monoclonal antibody specific for human NuMA, we followed the fate of human NuMA associated with microtubule asters upon dilution with a hamster mitotic extract. Consistent with in vivo data, this assay shows that NuMA can be displaced from the core of pre-assembled asters into the soluble pool. The half-time of NuMA displacement from asters under these conditions is ~5 minutes. Using this assay, we show that protein kinase activity and the NuMA-binding protein LGN regulate the dynamic exchange of NuMA on microtubule asters. Thus, the dynamic properties of NuMA are regulated by multiple mechanisms including protein phosphorylation and binding to the LGN protein, and the rate of exchange between soluble and microtubule-associated pools suggests that NuMA associates with an insoluble matrix at spindle poles.

Supplementary material available online at
http://jcs.biologists.org/cgi/content/full/117/26/6391/DC1

Key words: NuMA, Mitotic Spindle, Kinetochore, Microtubule, Centrosome

Introduction

Chromosome movement in both mitosis and meiosis is directed by a complex, microtubule-based structure called the spindle (Compton, 2000; Hyman and Karsenti, 1996; Rieder, 1991; Mitchison, 1989; McIntosh and Koonce, 1989). Microtubules within the spindle are arranged in a highly ordered and symmetrical bipolar array with minus ends focused at spindle poles. In vertebrate somatic cells, centrosomes are located at spindle poles, but a range of evidence indicates that centrosomes are neither necessary nor sufficient to focus microtubule minus ends at spindle poles. For example, functional bipolar spindles with focused spindle poles form after centrosomes are eliminated from cultured cells by laser ablation (Khodjakov et al., 2000). Moreover, microtubule focusing at spindle poles is disrupted by perturbation of the minus-end-directed motor cytoplasmic dynein despite the presence of centrosomes and their active nucleation of astral microtubule arrays (Heald et al., 1997; Gaglio et al., 1997). These and other results demonstrate that non-centrosomal proteins such as dynein are responsible for microtubule minus-end focusing at spindle poles and that these proteins drive spindle pole organization in the presence or absence of centrosomes (Compton, 1998).

One non-centrosomal protein that is essential for spindle pole organization is the large coiled-coil protein NuMA (Compton and Cleveland, 1994; Cleveland, 1995). NuMA localizes to the interphase nucleus and concentrates at the polar ends of the spindle in mitosis (Lyderson and Pettijohn, 1980; Price and Pettijohn, 1986; Compton et al., 1992; Kallajoki et al., 1991; Tousson et al., 1991; Yang et al., 1992; Maekawa et al., 1991). After nuclear envelope breakdown, during prometaphase, NuMA associates with cytoplasmic dynein and uses its minus-end-directed motor activity to accumulate at spindle poles (Merdes et al., 1996; Merdes et al., 2000), where it focuses microtubule minus ends and tethers centrosomes to the body of the spindle. NuMA has been shown to self-assemble into large matrices (Saredi et al., 1996; Saredi et al., 1997; Harborth et al., 1999; Gueth-Hallonet et al., 1998) and electron microscopy has demonstrated that, once NuMA localizes to spindle poles, it becomes part of an insoluble matrix closely associated with microtubule minus ends (Dionne et al., 1999). NuMA can cross-link microtubules in vitro (Haren and Merdes, 2002), suggesting that its essential

role in spindle pole organization is to form multivalent microtubule-binding matrices that cross-link microtubule minus ends at spindle poles.

Despite the wealth of information about the function of NuMA and the consequences to spindles when NuMA function is perturbed, little is known about the dynamics of NuMA at spindle poles. Indeed, there are two general models that explain how NuMA organizes microtubule minus ends at spindle poles, and these two models differ in the predictions they make about NuMA dynamics at spindle poles. One model postulates that NuMA forms a stable complex with cytoplasmic dynein and that these proteins rapidly cycle on and off microtubules to focus minus ends at spindle poles using the minus-end-directed motor activity of dynein. The other model posits that NuMA uses the motor activity of cytoplasmic dynein to become deposited at spindle poles, where it builds a matrix to hold microtubule minus ends together following dissociation from dynein. As a first step in distinguishing between these two models, we examined the dynamics of NuMA at spindle poles using both in vivo and in vitro methods. The results indicate that NuMA dynamically exchanges between soluble and spindle-associated pools, but the exchange is relatively slow compared with other spindle proteins. We also present evidence that multiple mechanisms regulate the exchange of NuMA between soluble and spindle-associated pools.

Materials and Methods

Cell culture

HeLa, BHK and NRK-52E cells (kindly provided by Y.-L. Wang, University of Massachusetts, Worcester, MA) were maintained in Dulbecco's modified Eagle's medium (DMEM) supplemented with 10% fetal calf serum. For transient expression of NuMA, NRK-52E cells were transformed by electroporation in suspension (three 5-millisecond pulses at 350 V s^{-1} m^{-1}). After electroporation cells were seeded on 24×24-mm number 1 coverslips in Petri dishes. For photobleaching experiments coverslips were mounted in Rose chambers in phenol-free L15 media supplemented with 10% fetal calf serum. Cells were kept at 37°C using a custom-built microscope stage heater (Rieder and Cole, 1998).

GFP-NuMA plasmid construction

To create the fusion between green fluorescent protein (GFP) and NuMA (GFP-NuMA), the cDNA encoding full-length human NuMA was amplified with Pfu Turbo DNA polymerase (Stratagene, La Jolla, CA) using forward (5′-ATGACACTCCACGCCACCCGG-3′) and reverse (5′-CTTGCCCTTGGCTCGAGGGG-3′) primers and inserted into the *Ecl*136II site of either pEGFP-N1 or pEGFP-C3 plasmids (BD Biosciences Clonetech, Palo Alto, CA). Each construct was verified by DNA sequencing.

Microscopy and FRAP

Multidimensional GFP fluorescence/differential interference contrast (DIC) time-lapse sequences were collected on a custom-modified Nikon TE-200, equipped with Orca II cooled CCD camera (Hamamatsu), *z*-axis piezoelectric positioner (Physik Instrumente), electronically controlled *xy*-axis stage (LEP), filter wheels (LEP) and shutters (Vincent Associates). The system was driven by Isee imaging software (Isee Imaging) run on O2 workstation (Silicon Graphics). NuMA signal associated with one of the two spindle poles (~2-3 μm in diameter) was photobleached during late prometaphase-metaphase by a brief (200-millisecond) pulse of 488-nm laser light directed through the lens. To capture the full in-focus intensity of the signal, full through-focus *z*-axis series of GFP images (background and flatfield corrected) were collected at each time point. Maximal-intensity projections were then calculated from these initial three-dimensional (3D) datasets and the signal from NuMA/GFP associated with each individual spindle pole was measured as previously described (Khodjakov and Rieder, 1999).

Images of microtubule asters were captured using an Orca II cooled CCD camera (Hamamatsu) mounted on a Zeiss Axioplan 2 microscope. Line scans were performed on unprocessed images using the advanced measurements tool of the Openlab software package (Improvision).

Immunological techniques

NRK-52E cells were permeabilized with 1% Triton X-100 in PEM buffer (100 mM PIPES, 5 mM EGTA, 2.5 mM $MgCl_2$, pH 6.9), and fixed with 1% glutaraldehyde in PEM. Polyclonal antibody against NuMA (Gaglio et al., 1995) was used at 1:200 dilution and visualized with Alexa-488-labeled goat anti-rabbit antibody (Molecular Probes). DNA was counterstained with Hoechst 33342 dye. Images were collected as 3D stacks (0.2 μm steps), deconvolved using DeltaVision 2.5 software (Applied Precision) and presented as maximal-intensity projections.

Microtubule asters were spread on poly-L-lysine-coated coverslips and fixed in –20°C methanol for 10 minutes. Microtubules and NuMA were visualized using mouse monoclonal antibody DM1α (Sigma, St Louis, MO) and a rabbit polyclonal against NuMA (Gaglio et al., 1995) followed by species-specific fluorescein isothiocyanate (FITC)- and Texas-Red-conjugated secondary antibodies (Vector labs, Burlingame, CA).

Cells transfected with control or GFP-NuMA plasmids were washed in PBS and total cell protein harvested directly into sodium-dodecyl-sulfate polyacrylamide-gel electrophoresis (SDS-PAGE) sample buffer. Proteins were separated by size and immunoblotted for NuMA using the rabbit polyclonal antibody as previously described (Gaglio et al., 1995).

Mitotic extracts

Mitotic extracts were prepared from both HeLa and BHK cells in KHMM buffer (78 mM KCl, 50 mM HEPES, pH 7.0, 4 mM $MgCl_2$, 1 mM $MnCl_2$, 2 mM EGTA, 1 mM dithiothreitol) using the previously described protocol (Gaglio et al., 1995). Extracts from BHK cells were fractionated on heparin-Sepharose (Sigma, St Louis, MO) and bound proteins were eluted with KHMM buffer containing 0.5 M NaCl. The elution fraction was then desalted into KHMM buffer using a PD-10 column (Amersham Biosciences). Following assembly of microtubule asters in human extracts the human extract was diluted at a 1:4 ratio with either KHMM buffer or the elution fraction of the BHK extract.

Results

NuMA dynamics at mitotic spindle poles

We first evaluated distributions of endogenous NuMA in fixed NRK-52E cells as a prerequisite for our NuMA-GFP expression studies (see below). Immunofluorescence staining reveals that NuMA, which is diffusely spread throughout the nucleus during interphase, begins to form aggregates at the earliest signs of prophase chromosome condensation (Fig. 1A,B). Initially small, these aggregates become larger and fewer in later prophase (Fig. 1C). In prometaphase cells, most NuMA is associated with spindle poles but individual NuMA aggregates can still be seen in the cytoplasm (Fig. 1D,E).

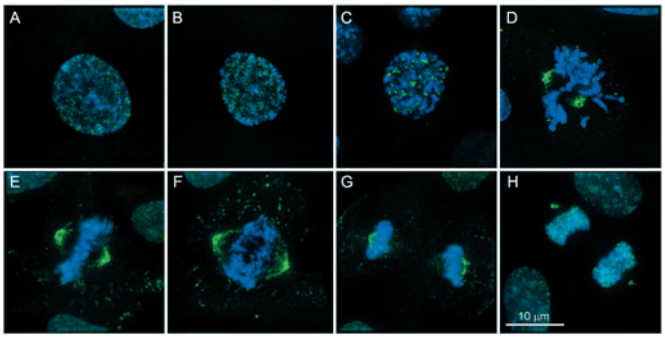

Fig. 1. Localization of endogenous NuMA in NRK 52E cells. (A) Early prophase. (B) Mid-prophase. (C) Late prophase. (D) Prometaphase. (E) Metaphase. (F) Anaphase. (G) Telophase. (H) Early G1. Immunostaining with anti-NuMA antibody (green), DNA is counterstained with Hoechst 33342. Maximal-intensity projections through the entire cell volume.

During late telophase, the amount of NuMA associated with spindle poles decreases significantly and, at the same time, accumulation of NuMA is seen in the forming daughter nuclei (Fig. 1G,H). However, it is noteworthy that, in these cells, a small amount of NuMA remains associated with double dots adjacent to each daughter nucleus for a significant time after reformation of the nuclear envelope (Fig. 1H).

To examine the dynamics of NuMA at spindle poles in living cells, we constructed a eukaryotic expression plasmid containing a cDNA encoding NuMA-GFP fusion protein. Immunoblot analysis with a NuMA-specific antibody of extracts from HeLa cells following transient transfection with this plasmid reveals both endogenous NuMA and the NuMA-GFP fusion protein (see Fig. S1 in supplementary material). The molecular weight of the fusion protein is consistent with the predicted molecular weight of NuMA plus GFP. Live-cell microscopy reveals that GFP-NuMA is confined inside of nuclei during interphase and associated with mitotic spindle poles during metaphase in several different cell types (e.g. PtK1, NRK-52E, CHO and HeLa cells). Furthermore, the course of mitosis appears to be normal in cells that expressed low to moderate amounts of GFP-NuMA. However, the brightest cells, which grossly overexpressed NuMA-GFP, exhibit several prominent abnormalities. First, during interphase, NuMA-GFP is seen to form a lattice within the nucleus. This lattice could not only be detected by fluorescence microscopy but also be seen as abnormal chromatin condensation in DIC images. Second, cells that grossly overexpress NuMA-GFP often form monopolar spindles with large accumulation of NuMA-GFP in the center of the spindle and multiple smaller aggregates of this protein in the peripheral parts of the cell. Because these observations are consistent with the expected phenotypes of overexpression of functional NuMA protein (Merdes et al., 2000; Gueth-Hallonet et al., 1998), we conclude that our NuMA-GFP fusion is functional. Furthermore, because the distribution of NuMA-GFP in cells expressing low to moderate levels of the fusion protein is indistinguishable from that of endogenous NuMA (Fig. 2; see Video S1 in supplementary material), we conclude that, at lower expression levels, our NuMA-GFP is a good indicator of the behavior of endogenous NuMA during the cell cycle.

Combined DIC/3D-fluorescence time-lapse recording of mitosis in NuMA/GFP-expressing cells allowed us to follow NuMA behavior with high spatial and temporal resolution, and revealed several new features of NuMA dynamics during mitosis. During interphase, NuMA is homogeneously spread through the nucleus. The only nuclear volume that prominently lacks NuMA is the nucleolus (Fig. 2A). Thus, before prophase, NuMA distribution is indistinguishable from that of chromatin. As cells enter prophase, NuMA begins to aggregate, initially forming hundreds of small (below the resolution limit of light microscopy) aggregates. Surprisingly, these aggregates are highly motile inside the nucleus. Many of the aggregates are seen to move up to 1.5 μm in 30 seconds, which corresponds to a 3 μm minute^{-1} velocity. This motion could not be mediated by microtubules because it occurs within the nucleus before nuclear envelope breakdown. In many cases, two granules moved towards each other and then coalesce into a single, larger aggregate (Fig. 3D,E). The intranuclear motion and fusion result in the formation of just a few large aggregates (up to 2.5 μm in diameter) by late prophase (Fig. 3; see Videos 2,3 in supplementary material) that are clearly separated from the emerging chromosomes. These aggregates are similar to those seen in untransfected cells (Fig. 1), although they are somewhat larger, which might result from the exogenous expression of GFP-NuMA.

Intranuclear movement of NuMA aggregates continues throughout prophase until nuclear envelope breakdown. As soon as microtubules begin to penetrate the nuclear volume, the character of NuMA mobility changes dramatically. The NuMA aggregates are now seen to stream on microtubules towards the centrosomes (Fig. 4; see Video 3 in supplementary material). During streaming, the aggregates stretch along the

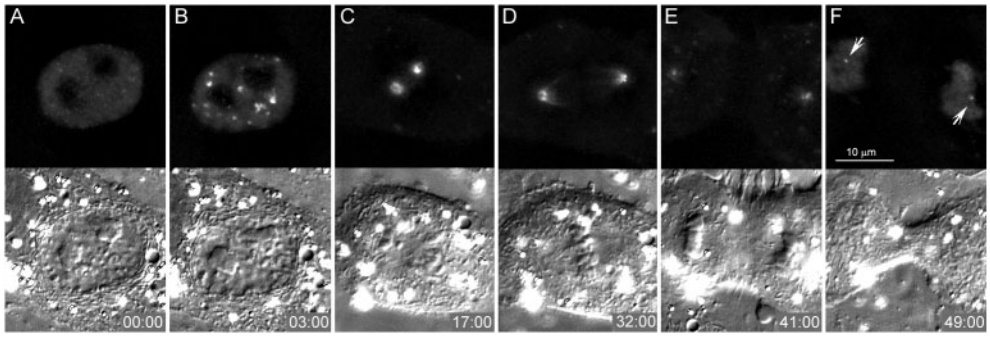

Fig. 2. Behavior of GFP-NuMA in NRK52E cells. Selected frames from combinational 3D fluorescence (top half of each frame) / DIC (bottom half of each frame) time-lapse recording of an individual cell. (A) Early prophase. (B) Mid-prophase. (C) Prometaphase. (D) Anaphase onset. (E) Telophase. (F) Cytokinesis. Notice that the distribution of GFP-NuMA closely matches that of endogenous NuMA in the same cell type at all stages of mitosis (Fig. 1). Arrows in (F) indicate doubled NuMA-positive dots that remain visible in most cells during earlier G1. Time in minutes:seconds.

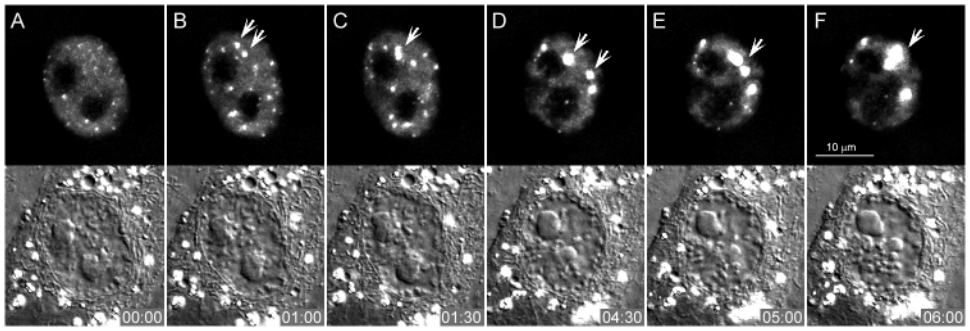

Fig. 3. Intranuclear movements of GFP-NuMA during prophase in NRK 52E cells. (Same cell as in Fig. 2.) This sequence highlights NuMA movements as the cell progresses through late prophase. Selected frames from combinational 3D fluorescence (top half of each frame) / DIC (bottom half of each frame) time-lapse recording of an individual cell. (A-C) Early prophase, (D-E) late prophase. Notice that NuMA aggregates move inside of the nucleus, which still has intact nuclear envelope as revealed by DIC (bottom of each frame). Many NuMA aggregates are seen to move directly towards each other and then fuse (arrows in B,C and D,F). Time in minutes:seconds.

microtubule (or microtubule bundle) and form a continuous ribbon. Because the temporal resolution of our 3D record is limited to 30 seconds, we are unable to determine the exact velocity of the microtubule-mediated movement of NuMA aggregates. However, we can state that it exceeds 15 μm minute^{-1}, consistent with previous descriptions of polewards transport of NuMA (Merdes et al., 2000).

As the result of microtubule-mediated streaming, the great majority of NuMA aggregates become incorporated into the forming spindle poles within just a few minutes (~2-3 minutes) after nuclear envelope breakdown. However, individual aggregates can be seen to become 'lost' in the peripheral areas of the cell many micrometers away from spindle poles. These aggregates exhibit Brownian-type movements until they suddenly stretch and stream towards one of the spindle poles (Fig. 4E,F). This kind of behavior is consistent with the classic 'search-and-capture' role of microtubule asters and probably indicates that NuMA aggregates move polewards whenever they encounter a microtubule (or a microtubule bundle). This incorporation of peripheral NuMA aggregates into the spindle poles continues through mid-anaphase (see Videos 1,3 in supplementary material).

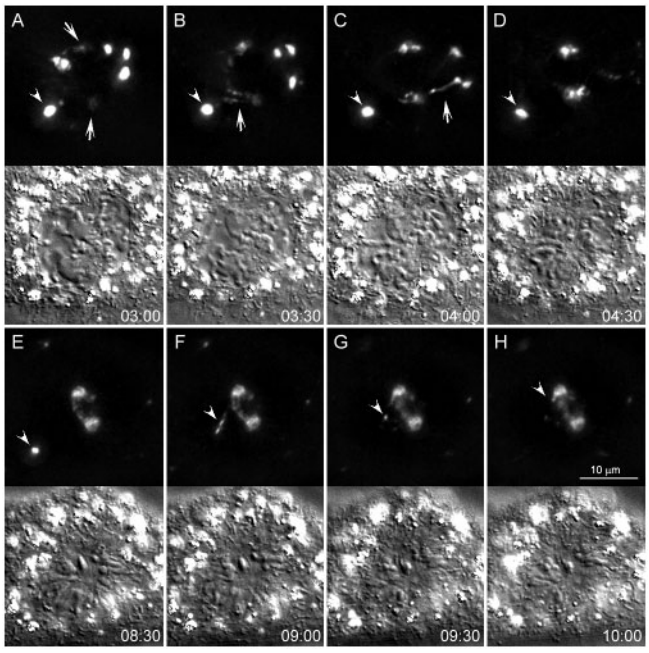

Fig. 4. Polewards transport of GFP-NuMA. Similar to Fig. 3 except that this sequence focuses on NuMA movements after nuclear envelope breakdown (NEB). (A) At NEB, the separated centrosomes (arrows) do not contain appreciable amounts of NuMA. However, immediately after NEB, NuMA begins to 'stream' towards the centrosomes (B,C, arrows). (D) Within 2-3 minutes of NEB, most NuMA becomes associated with the forming spindle poles. However, some NuMA aggregates can persist in the peripheral parts of the cell for much longer (A-E, arrowhead). These aggregates gradually decrease in size until they suddenly 'stream' toward one of the spindle poles (arrowhead in F-H).

Concurrent with polewards transport and incorporation into spindle poles, peripheral NuMA aggregates exhibit prominent changes in size that do not appear to be microtubule dependent. Most of the large aggregates that are present in cells immediately after nuclear envelope breakdown continuously decrease in apparent size and signal intensity as cells progress through prometaphase (Fig. 4A-E, arrowhead). This phenomenon implies that NuMA is in dynamic exchange between the aggregates and a soluble pool, and that NuMA is dissociating from the aggregates independently of microtubule-mediated transport. This is an important feature because it suggests that NuMA within spindle poles might also undergo similar dynamics.

To determine parameters and the nature of NuMA dynamics within the spindle pole, we photobleached the NuMA-GFP signal associated with one of the two spindle poles during mid-prometaphase and then followed the dynamics of fluorescence recovery after photobleaching (FRAP). We found that NuMA-GFP signal consistently recovers in the photobleached pole (Fig. 5). However, the level of recovery is different in different cells. One complication that we encountered while analysing the results of our initial FRAP experiments is that, in cells with prominent peripheral NuMA aggregates, the character of FRAP curves is greatly affected by the unpredictable incorporation of new NuMA-GFP aggregates via microtubule-mediated transport. We then limited our FRAP experiments to cells that expressed minimally detectable levels of NuMA-GFP and conducted photobleaching only after large peripheral NuMA aggregates had been incorporated into the spindle poles. We also normalized the results of the measured intensity of the photobleached poles with respect to the intensity to the control, non-irradiated pole. The normalization allowed us to compensate for the natural reduction in the pole-associated

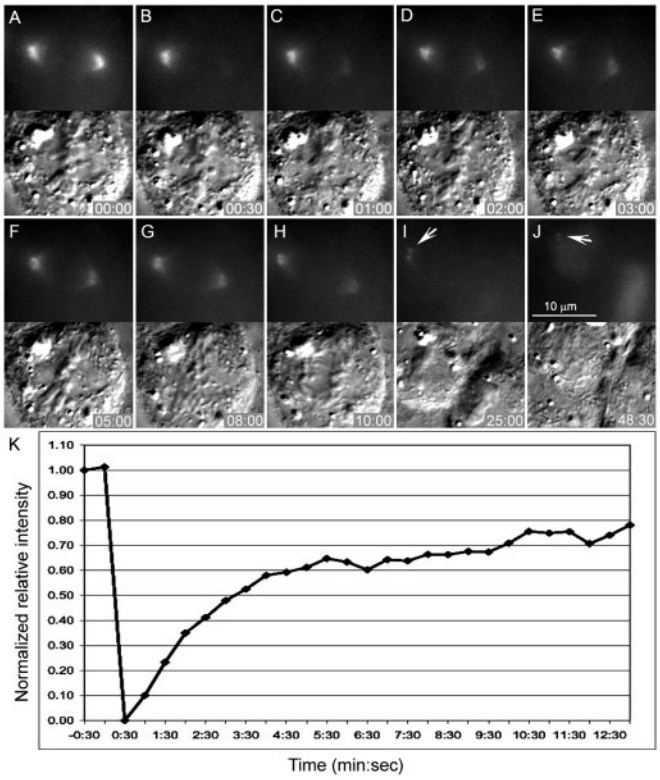

Fig. 5. Dynamic exchange of pole-associated NuMA/GFP revealed by fluorescence recovery after photobleaching. (A-J) Selected frames from combinational time-lapse recording (similar to Figs 2-4). NuMA associated with one of the two spindle poles during late prometaphase was photobleached (A,B) by a 200 millisecond pulse of 488-nm laser light. The photobleached signal gradually recovered, whereas the intensity of the non-photobleached control pole decreased over time (C-H). Notice that the cytoplasmic double dots of NuMA that are seen in association with the control pole (I,J, arrow) did not appear in the photobleached pole. (K) Normalized intensity of NuMA-GFP fluorescence associated with the irradiated spindle pole over time.

NuMA-GFP signal that occurs during the second half of mitosis. A typical normalized FRAP curve is shown in Fig. 5K.

Our FRAP experiments reveal several interesting features of pole-associated NuMA dynamics. First, FRAP shows that a bulk of NuMA is in constant dynamic exchange with the soluble pool and 50% of the original signal recovers within 208±41 seconds (n=13). However, in most cells, signal recovery of the irradiated pole did not reach more then 80-85% of the prebleached normalized intensity and 50% of that level was recovered in 176±46 seconds (n=13). This indicates that there are two distinct populations of NuMA within a spindle pole – a major population that undergoes continuous dynamic exchange and a minor population that is more stably bound. The presence of the second population is also apparent upon analysis of images of the photobleached cells. We noticed that, as the NuMA-GFP signal diminishes within the pole during telophase, it always remains present in two sharp dots (Fig. 5I,J). This residual signal persists through completion of cytokinesis and well into the ensuing G_1 phase. Importantly, this association of NuMA with doubled dots is also seen in

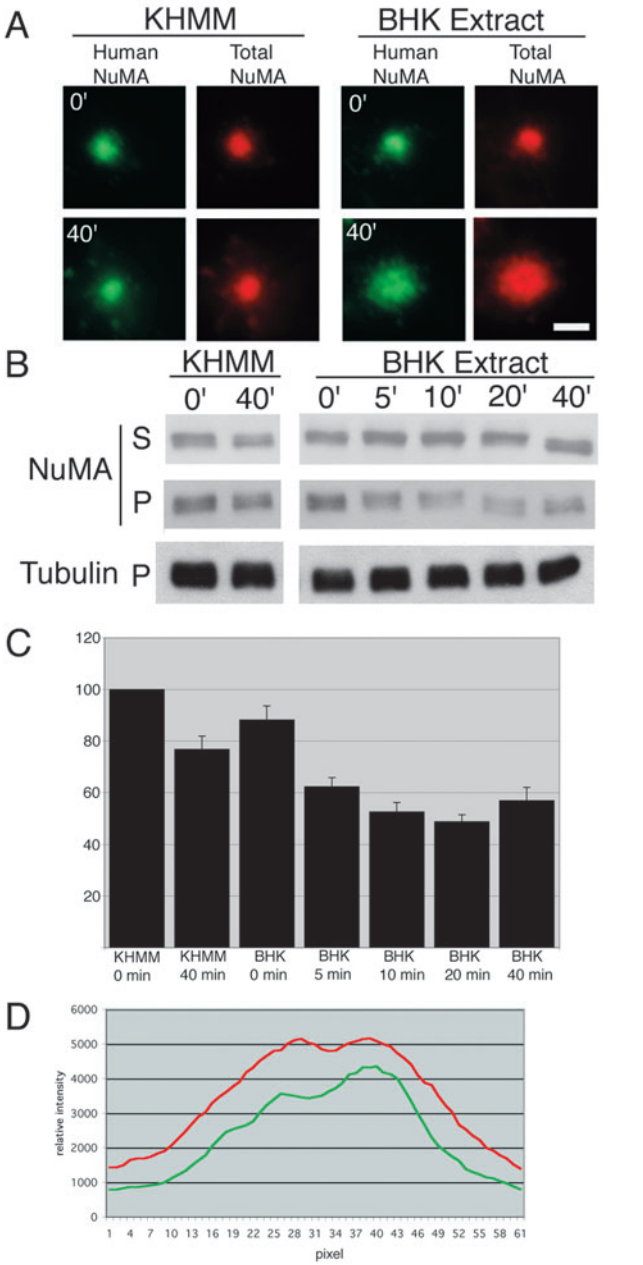

Fig. 6. Dynamic exchange of NuMA on microtubule asters. (A) Indirect immunofluorescence images of microtubule asters using a human NuMA-specific monoclonal antibody (Human NuMA) and a rabbit polyclonal antibody that recognizes both human and hamster NuMA (Total NuMA) immediately (0′) or 40 minutes (40′) after mixing with either buffer alone (KHMM) or hamster mitotic extract (BHK Extract). (B) Extracts were separated into 10,000 ***g*** soluble (S) or insoluble (P) fractions and immunoblotted with a human NuMA-specific monoclonal antibody and tubulin-specific antibody at various times (indicated in minutes) following dilution with either buffer alone (KHMM) or hamster mitotic extract (BHK Extract). (C) The proportion of human NuMA in the pellet fraction was determined using densitometry of immunoblots from three independent trials and is normalized to 100% using the 0-minute time point following dilution in KHMM buffer alone. Values represent the average and standard deviation. (D) Fluorescent images from the 40-minute time point were scanned with a horizontal line 1 pixel wide. Pixel intensities for both human NuMA (green) and total NuMA (red) are shown. Scale bar, 2 μm.

non-irradiated NuMA/GFP-expressing cells (see Video 1 in supplementary material) and in untransfected NRK-52E cells immunostained for endogenous NuMA (Fig. 1H). The appearance and behavior of the NuMA-positive dots is consistent with that of centrioles. Thus, our data suggest that a portion of the non-exchangeable fraction of NuMA is associated directly with the centrosome.

Regulation of NuMA dynamics on microtubule asters in vitro

Thus far, our results indicated that a significant proportion of NuMA constantly exchanges between soluble and spindle-associated pools during mitosis. However, these results are complicated by dynamic microtubules that constantly search the cytoplasm and facilitate capture and transport of NuMA to poles. To circumvent this problem, we exploited mammalian mitotic extracts in which NuMA is essential for the formation of microtubule asters (Gaglio et al., 1995). Microtubule asters formed in these extracts lack microtubule dynamics because microtubules are stabilized by the addition of Taxol. For this assay, we assembled microtubule asters in a mitotic extract prepared from human HeLa cells. We then added a mitotic extract prepared from hamster BHK cells and followed the fate of human NuMA associated with asters by indirect immunofluorescence microscopy and immunoblotting using a monoclonal antibody specific for the human NuMA protein (Fig. 6). To prevent de novo aster assembly in the hamster extract in this assay, we fractionated the hamster BHK extract on a heparin-Sepharose column before addition to the human HeLa cell extract. Under the buffer conditions used to make these extracts, tubulin emerges in the flow-through fraction from this column and all other known aster-associated proteins (e.g. NuMA, HSET, Eg5, dynein, dynactin, TPX2) bound to the column and are recovered in an elution fraction. We used the elution fraction for this experiment because it possessed NuMA and other proteins involved in aster assembly but is incapable of microtubule aster assembly owing to the lack of tubulin (data not shown).

As a control for this experiment, we diluted the human mitotic extract containing pre-assembled microtubule asters into buffer alone. Immunofluorescence microscopy demonstrates that NuMA remained tightly focused at the core of microtubule asters both immediately following dilution (time=0′) and 40 minutes after dilution (Fig. 6A). Immunoblots of the soluble and aster-containing insoluble fractions demonstrate only a 20-25% decrease in the proportion of NuMA associated with asters 40 minutes after dilution with KHMM buffer (Fig. 6B,C). Thus, microtubule asters are stable to dilution in buffer alone and most NuMA remains associated with pre-assembled asters following dilution with KHMM buffer.

A significant change in the distribution of human NuMA on asters is observed upon dilution of human HeLa extracts containing pre-assembled asters with hamster BHK extract. Immunofluorescence microscopy shows human NuMA tightly

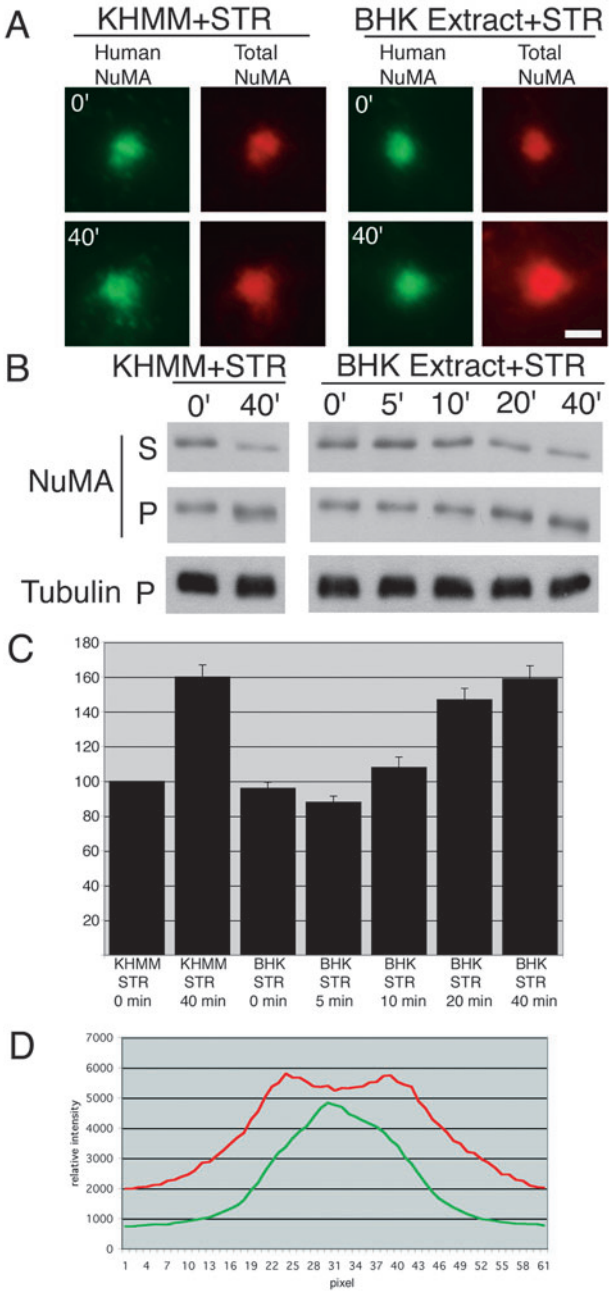

Fig. 7. Staurosporine inhibits the dynamic exchange of NuMA on microtubule asters. (A) Indirect immunofluorescence images of microtubule asters using a human NuMA-specific monoclonal antibody (Human NuMA) and a rabbit polyclonal antibody that recognizes both human and hamster NuMA (Total NuMA) immediately (0′) or 40 minutes (40′) after mixing with either buffer alone (KHMM+STR) or hamster mitotic extract (BHK Extract+STR). (B) Extracts were separated into 10,000 ***g*** soluble (S) or insoluble (P) fractions and immunoblotted with a human NuMA-specific monoclonal antibody and a tubulin-specific antibody at various times (indicated in minutes) following dilution with either buffer alone (KHMM+STR) or hamster mitotic extract (BHK Extract+STR). (C) The proportion of human NuMA in the pellet fraction was determined using densitometry of immunoblots from three independent trials and is normalized to 100% using the 0-minute time point in following dilution in KHMM buffer alone. Values represent the average and standard deviation. (D) Fluorescent images from the 40-minute time point were scanned with a horizontal line 1 pixel wide. Pixel intensities for both human NuMA (green) and total NuMA (red) are shown. Scale bar, 2 μm.

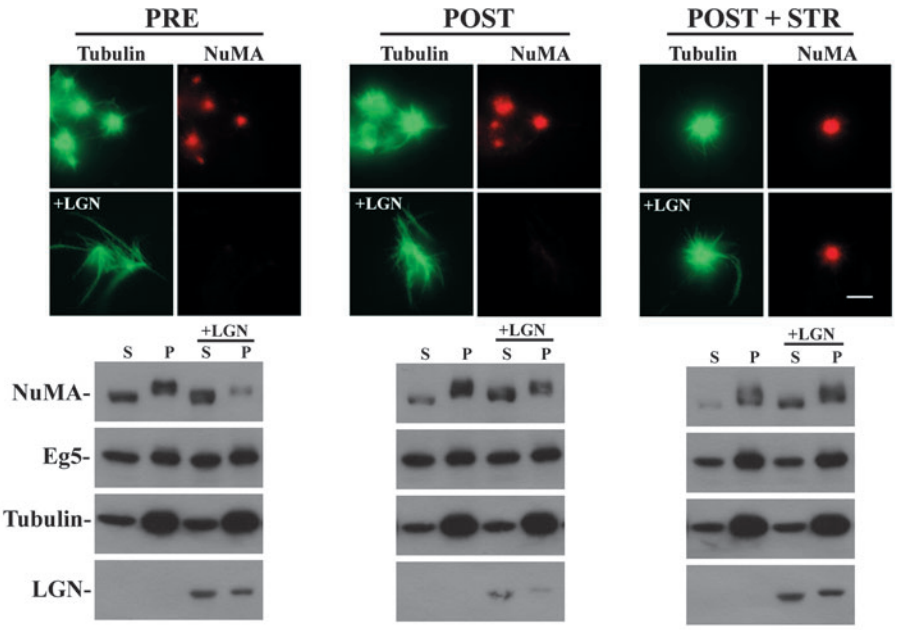

Fig. 8. LGN displaces NuMA from microtubule asters. (top) Indirect immunofluorescence images of microtubule arrangements in untreated extracts or extracts to which LGN has been added (+LGN). The LGN protein was added to samples before microtubule aster assembly (PRE), after microtubule aster assembly (POST) or after microtubule aster assembly along with staurosporine (POST+STR). (bottom) Extracts were separated into 10,000 ***g*** soluble (S) and insoluble (P) fractions, separated by size by SDS-PAGE and immunoblotted with antibodies specific to NuMA, Eg5, tubulin and LGN, as indicated. Scale bar, 5 μm.

focused at aster cores immediately after dilution (time=0′), as expected. However, 40 minutes after dilution, human NuMA is more diffusely localized on asters and occupies a larger area (Fig. 6A). Immunoblots of the soluble and aster-containing insoluble fractions demonstrate a significant decrease in the quantity of human NuMA in the aster-containing pellet fraction (Fig. 6B). Diminution in the quantity of human NuMA associated with pre-assembled asters maximized at 20 minutes after dilution with hamster BHK extract, and the time to reach half-maximum is ~5 minutes (Fig. 6C). At the 20 minute time point, the quantity of human NuMA associated with asters is reduced ~50% relative to the initial time point. Importantly, there was no significant change in the quantity of tubulin in the insoluble fraction (Fig. 6B), indicating that changes in NuMA distribution were not caused by alterations in the amount of microtubule polymer. Thus, a significant proportion of NuMA shifts to the soluble pool following dilution with hamster BHK extract but not buffer alone, consistent with the exchange of NuMA at spindle poles revealed by FRAP analyses. The kinetics of release of NuMA from pre-assembled asters are slightly slower than the dynamics of NuMA measured in living cells by FRAP, but this difference is minor considering the significant differences in concentrations and temperature that exist between in vitro and in vivo conditions. Also, the extent of release of NuMA is less than observed in living cells by FRAP but this might reflect either an non-exchangeable pool of NuMA on microtubule asters in vitro or the technical limitations of this extract mixing regime.

NuMA displays mitosis-specific phosphorylation (Price and Pettijohn, 1986; Compton and Luo, 1995; Gaglio et al., 1995; Sparks et al., 1995; Saredi et al., 1997) and we used the extract mixing assay to test whether the dynamic behavior of NuMA is regulated by protein phosphorylation. For this experiment, we assembled microtubule asters in human HeLa extracts and then added both hamster BHK extract and the protein-kinase inhibitor staurosporine (1 μM). We then followed the fate of human NuMA associated with asters by indirect immunofluorescence microscopy and immunoblotting using a monoclonal antibody specific for the human NuMA protein (Fig. 7). As a control, we diluted human HeLa extract containing pre-assembled microtubule asters into buffer alone in the presence of staurosporine. Microtubule asters are stable when diluted in buffer containing staurosporine and NuMA remains tightly focused at aster cores (Fig. 7A). Immunoblots of the soluble and aster-containing insoluble fractions demonstrate an increase in the quantity of NuMA on asters after 40 minutes (Fig. 7B,C), indicating that staurosporine treatment alone is sufficient to shift NuMA from the soluble pool to the aster-associated pool. This trend is also observed when human HeLa extract containing pre-assembled asters is diluted with hamster BHK extract in the presence of staurosporine. Human NuMA remained tightly focused at aster cores (Fig. 7A) and the quantity of human NuMA associated with asters increases over time, reaching a maximum at 40 minutes (Fig. 7B,C). As in the previous experiment, there was no significant change in the quantity of tubulin in the insoluble fraction (Fig. 7B), indicating that changes in NuMA distribution caused by inhibition of protein kinase activity were not caused by alterations in the amount of microtubule polymer. These results demonstrate that protein kinase activity is required to determine the steady-state distribution of NuMA in a mitotic extract, and that inhibition of protein kinase activity shifts the steady-state distribution of NuMA to being predominantly aster associated.

The extract mixing assay used a 4:1 ratio of hamster to human mitotic extracts. Under these conditions, most NuMA recruited to asters after extract mixing will be of hamster origin. If NuMA is free to exchange between soluble and aster-associated pools then the tightly focused core of NuMA on pre-assembled asters should disperse and the human and hamster proteins should homogenize in the extract. Thus, the distribution of human and hamster proteins should be similar as demonstrated by line scans across the aster core at the 40-minute time point (Fig. 6D). By contrast, if the release of NuMA from pre-assembled asters is suppressed by inhibition of protein kinase activity then the tightly focused core of human NuMA on pre-assembled asters should be stabilized. Any NuMA that is subsequently recruited to asters under these conditions will be predominantly hamster NuMA and will accumulate on the exterior of the pre-assembled aster core,

forming a ring as seen by line scans across the aster core at the 40 minute time point (Fig. 7D).

Based on these results, we hypothesize that exogenously added recombinant LGN protein will disrupt pre-assembled microtubule asters. LGN is related to *Drosophila* Pins and has been shown to bind directly to NuMA at a site that overlaps NuMA's microtubule binding site (Du et al., 2001; Du et al., 2002). We reasoned that the dynamic cycling of NuMA on and off microtubule asters would render it accessible to LGN, creating conditions under which LGN would compete with microtubules for NuMA binding. To test this hypothesis, we added recombinant LGN to the mitotic extract before and after microtubule aster assembly (Fig. 8). Addition of recombinant LGN to the mitotic extract before microtubule aster assembly has no detectable effect on the efficiency of either microtubule polymerization or Eg5 association with microtubules, but significantly reduces the efficiency with which NuMA associated with microtubules. Consequently, microtubules fail to organize into asters (Fig. 8, PRE). Similarly, the addition of LGN to a mitotic extract containing pre-assembled asters has no detectable effect on the efficiency of microtubule polymerization and Eg5 association with microtubules, but reduces the efficiency with which NuMA associated with microtubules. Consequently, pre-assembled microtubule asters lose their tight focus and disperse (Fig. 8, POST). Protein-kinase activity is required for LGN to compete NuMA off microtubules, because there is no detectable change in either the distribution of NuMA or the organization of microtubule asters if staurosporine is added along with LGN (Fig. 8, POST+STR). Thus, the dynamic exchange of NuMA between soluble and aster-associated pools permits added LGN to act as a competitive inhibitor for NuMA association with microtubules.

Discussion

Using both in vivo and in vitro methods, we examined the behavior of NuMA at spindle poles during mitosis. Despite inherent technical differences, each method reveals the same outcome – there are three distinct pools of NuMA in mitotic cells. One pool of NuMA is associated with spindle poles and does not undergo significant exchange with the other two pools. Analyses of GFP-NuMA in living cells indicate that this pool constitutes <20% of total NuMA and that a portion of this pool is associated with centrosomes in the particular cells examined here. The second pool of NuMA is also spindle associated, but this pool readily exchanges with the third pool of freely soluble NuMA. The average half-time for dynamic exchange between these latter pools is ~3 minutes (in vivo) or 5 minutes (in vitro). These two values are remarkably similar considering the significant differences between the techniques used to obtain them. This suggests that the underlying mechanisms regulating dynamic exchange of NuMA at spindle poles are robust to different experimental conditions.

NuMA has been shown to associate with both microtubules and itself, forming matrix-like arrays that cross-link microtubule minus ends at spindle poles (Haren and Merdes, 2002; Harborth et al., 2000; Gueth-Hallonet et al., 1999; Saredi et al., 1996; Saredi et al., 1997; Dionne et al., 1999). Thus, the exchange of NuMA between the soluble and spindle-associated pools requires the formation and breakage of multiple molecular interactions. One such interaction is the association of NuMA with cytoplasmic dynein that facilitates the accumulation of NuMA at spindle poles through minus-end-directed motor activity (Merdes et al., 1996; Merdes et al., 2000). However, we feel that the dynamic exchange of NuMA does not strictly require NuMA binding to dynein, and that diffusion-based mechanisms are likely to contribute to NuMA deposition at poles. Evidence to support this view comes from the images demonstrating that large aggregates of NuMA disassemble through microtubule-independent means (arrowhead, Fig. 4A-E), and that NuMA functionally contributes to microtubule aster formation in vitro in the absence of dynein (Gaglio et al., 1996). Thus, dynein-mediated transport of NuMA and diffusion-based exchange of NuMA at spindle poles are distinct processes occurring simultaneously. The superimposition of these processes probably explains why the recovery times after photobleaching observed here, measured after the completion of the transport of large NuMA aggregates was completed, were longer than those reported previously (Stenoien et al., 2003).

NuMA has been shown to undergo mitosis-specific phosphorylation (Price and Pettijohn, 1986; Compton and Luo, 1995; Gaglio et al., 1995; Sparks et al., 1995; Saredi et al., 1997), and we present data using the in vitro assay indicating that protein phosphorylation regulates the dynamic exchange of NuMA at spindle poles. That inhibition of protein-kinase activity shifts the steady-state distribution of NuMA in favor of aster association suggests that NuMA phosphorylation either promotes microtubule (and/or self) dissociation or prevents NuMA association with microtubules (and/or itself). The obvious corollary to this is that NuMA dephosphorylation catalysed by protein phosphatases either promotes microtubule (and/or self) association or prevents NuMA dissociation from microtubules (and/or itself). Consistent with this view, we have previously demonstrated that phosphorylation regulates the assembly of NuMA matrices in mitotic extracts (Saredi et al., 1997), and addition of protein phosphatase inhibitors to the mitotic extract shifts the steady-state distribution of NuMA in favor of the soluble pool, which blocks microtubule organization into asters and induces the disassembly of preformed asters (data not shown). Thus, the steady-state distribution of the exchangeable pool of NuMA is regulated by the balanced activities of protein kinases and phosphatases in mitosis. These data explain why recovery after photobleaching of GFP-NuMA at spindle poles in living cells is blocked when cellular energy is depleted using azide/deoxyglucose or delayed when protein kinases are inhibited with staurosporine (see Fig. S2 in supplementary material). The delay in recovery of photobleached GFP-NuMA at spindle poles induced by staurosporine treatment was minimal, but that is probably because staurosporine is toxic and we had to perform this experiment at the lower end of effective concentrations (100 nM). Alternatively, in living cells, the concentration of staurosporine used might preferentially inhibit the polewards transport of NuMA mediated by dynein and not significantly affect the diffusion-based exchange. Such a preferential inhibition would reduce but not eliminate exchange, as observed.

The identities of the kinases and phosphatases that act on NuMA are currently not well defined. Evidence suggests that Cdc2/Cyclin-B might play a role in regulating NuMA dynamics during mitosis. Specifically, mutation of the

predicted Cdc2/Cyclin-B phosphorylation sites blocks NuMA association with spindles (Compton and Luo, 1995) and Cdc2/Cyclin-B activity is necessary for NuMA-dynein association in frog egg extracts (Gehmlich et al., 2004). However, none of the previous experiments showed that Cdc2/Cyclin-B acts directly on NuMA, leaving open the possibility that it activates downstream kinases that directly phosphorylate NuMA. Moreover, NuMA's transition from the nuclear matrix to the spindle poles is a multistep process and we feel that it is likely that more than one protein kinase (and phosphatase) is involved in regulating those events.

In addition to phosphorylation, we show that the LGN protein regulates NuMA dynamics at spindle poles. LGN binds to NuMA at a site that overlaps with the microtubule binding site (Du et al., 2002) indicating that the added LGN protein acts as a competitive inhibitor of NuMA association with spindle microtubules. This view is consistent with LGN preventing microtubule aster formation and inducing the disassembly of preformed asters as it prevents the reassociation of NuMA with asters following its dissociation. This view also fits recent results examining LGN function in living cells. Overexpression of LGN displaced NuMA from spindles and spindle poles splayed apart (Du et al., 2001). Conversely, RNA-interference-induced knockdown of LGN levels led to a significant number of cells with multipolar spindles, which, based on the current results, form as a result of exaggerated quantities of NuMA binding to spindle microtubules (Du et al., 2001). These data demonstrate that the ratio of LGN to NuMA must be carefully regulated in mitotic cells. One mechanism of regulation is phosphorylation, because inhibition of protein-kinase activity prevented LGN from competitively inhibiting NuMA. Unfortunately, the current data do not indicate whether NuMA alone or both NuMA and LGN are the targets of this phosphorylation.

Finally, the rate of exchange of NuMA at spindle poles (half-time of 3-5 minutes) is rather slow and comparable to that measured for the turnover of tubulin subunits in kinetochore fibers (~7 minutes) (Zhai et al., 1995). Despite the similarity in exchange rates, it is unlikely that the turnover of NuMA and tubulin subunits are functionally linked in spindles because NuMA exchange was detected in the cell-free system in which Taxol is used to suppress microtubule dynamics. The exchange rates of NuMA measured here are significantly lower than other spindle-associated proteins for which exchange rates have been measured. For example, the microtubule-associated proteins MAP2 and MAP4 exchange on and off microtubules during mitosis with half-times of 14 seconds and 17 seconds, respectively (Olmsted et al., 1989). Also, Eg5 and Mad2 (two proteins essential for spindle assembly and function) have been shown to have half-times of exchange of <55 seconds (Kapoor et al., 2001) and 24-28 seconds (Howell et al., 2000), respectively. The exchange rate for Mad2 is particularly noteworthy because it is transported to spindle poles by cytoplasmic dynein (Howell et al., 2001). The facts that the polewards transport of both NuMA and Mad2 is facilitated by the minus-end-directed motor activity of dynein but the half-times of NuMA and Mad2 turnover at poles differ approximately tenfold clearly demonstrate that NuMA lingers at spindle poles following delivery by dynein. Thus, we interpret these data as indicating that the minus-end-directed motor activity of dynein facilitates the accumulation of NuMA at spindle poles, but that the two dissociate as NuMA is deposited in a matrix that forms by its interactions with itself and microtubule minus ends. The subsequent dynamics of this NuMA matrix is diffusion based and is regulated independently of further dynein-mediated transport through various mechanisms including phosphorylation and LGN binding. In this context, we would expect the dynamic exchange of dynein or its associated complex dynactin to be much more rapid than that of NuMA measured here.

This work was supported by grants from the NIH to D.A.C. (GM51542), I.M. (GM070902), and A.K. (GM59363).

References

Cleveland, D. W. (1995). NuMA involvement in nuclear structure, spindle assembly, and nuclear reformation. *Trends Cell Biol.* **5**, 60-64.

Compton, D. A. (1998). Focusing on spindle poles. *J. Cell Sci.* **111**, 1477-1481.

Compton, D. A. (2000). Spindle assembly in animal cells. *Annu. Rev. Biochem.* **69**, 95-114.

Compton, D. A. and Cleveland, D. W. (1994). NuMA, a nuclear protein involved in mitosis and nuclear reformation. *Curr. Opin. Cell Biol.* **6**, 343-346.

Compton, D. A. and Luo, C. (1995). Mutation of the predicted $p34^{cdc2}$ phosphorylation sites in NuMA impair the assembly of the mitotic spindle and block mitosis. *J. Cell Sci.* **108**, 621-633.

Compton, D. A., Szilak, I. and Cleveland, D. W. (1992). Primary structure of NuMA, an intranuclear protein that defines a novel pathway for the segregation of proteins in mitosis. *J. Cell Biol.* **116**, 1395-1408.

Dionne, M. A., Howard, L. and Compton, D. A. (1999). NuMA is a component of an insoluble matrix at mitotic spindle poles. *Cell Motil. Cytoskeleton* **42**, 189-203.

Du, Q., Stukenberg, P. T. and Macara, I. G. (2001). A mammalian partner of inscuteable binds NuMA and regulates mitotic spindle organization. *Nat. Cell Biol.* **3**, 1069-1075.

Du, Q., Taylor, L., Compton, D. A. and Macara, I. G. (2002). LGN blocks the ability of NuMA to bind and stabilize microtubules: a mechanism for mitotic spindle assembly regulation. *Curr. Biol.* **12**, 1928-1933.

Gaglio, T., Saredi, A. and Compton, D. A. (1995). NuMA is required for the organization of microtubules into aster-like mitotic arrays. *J. Cell Biol.* **131**, 693-708.

Gaglio, T., Saredi, A., Bingham, J. B., Hasbani, M. J., Gill, S. R., Shroer, T. A. and Compton, D. A. (1996). Opposing motor activities are required for the organization of the mammalian mitotic spindle pole. *J. Cell Biol.* **135**, 399-414.

Gaglio, T., Dionne, M. A. and Compton, D. A. (1997). Mitotic spindle poles are organized by structural and motor proteins in addition to centrosomes. *J. Cell Biol.* **138**, 1055-1066.

Gehmlich, K., Haren, L. and Merdes, A. (2004). Cyclin B degradation leads to NUMA release from dynein/dynactin and from spindle poles. *EMBO Rep.* **5**, 97-103.

Gueth-Hallonet, C., Wang, J., Harborth, J., Weber, K. and Osborn, M. (1998). Induction of a regular nuclear lattice by overexpression of NuMA. *Exp. Cell Res.* **243**, 434-452.

Harborth, J., Wang, J., Gueth-Hallonet, C., Weber, K. and Osborn, M. (1999). Self assembly of NuMA: multiarm oligomers as structural units of a nuclear lattice. *EMBO J.* **18**, 1689-1700.

Haren, L. and Merdes, A. (2002). Direct binding of NuMA to tubulin is mediated by a novel sequence motif in the tail domain that bundles and stabilizes microtubules. *J. Cell Sci.* **115**, 1815-1824.

Heald, R., Tournebize, R., Haberman, A., Karsenti, E. and Hyman, A. A. (1997). Spindle assembly in *Xenopus* extracts: respective roles of centrosomes and microtubule self-organization. *J. Cell Biol.* **138**, 615-628.

Howell, B. J., Hoffman, D. B., Fang, G., Murray, A. W. and Salmon, E. D. (2000). Visualization of Mad2 dynamics at kinetochores, along spindle fibers, and at spindle poles in living cells. *J. Cell Biol.* **150**, 1233-1249.

Howell, B. J., McEwen, B. F., Canman, J. C., Hoffman, D. B., Farrar, E. M., Rieder, C. L. and Salmon, E. D. (2001). Cytoplasmic dynein/dynactin drives kinetochore protein transport to the spindle poles and has a role in mitotic spindle checkpoint activation. *J. Cell Biol.* **155**, 1159-1172.

Hyman, A. A. and Karsenti, E. (1996). Morphogenetic properties of microtubules and mitotic spindle assembly. *Cell* **84**, 401-410.

Kallajoki, M., Weber, K. and Osborn, M. (1991). A 210 kDa nuclear matrix protein is a function part of the mitotic spindle; a microinjection study using SPN monoclonal antibodies. *EMBO J.* **10**, 3351-3362.

Kapoor, T. M. and Mitchison, T. J. (2001). Eg5 is static in bipolar spindles relative to tubulin: evidence for a static spindle matrix. *J. Cell Biol.* **154**, 1125-1133.

Khodjakov, A. and Rieder, C. L. (1999). The sudden recruitment of gamma-tubulin to the centrosome at the onset of mitosis and its dynamic exchange throughout the cell cycle, do not require microtubules. *J. Cell Biol.* **146**, 585-596.

Khodjakov, A., Cole, R. W., Oakley, B. R. and Rieder, C. L. (2000). Centrosome-independent mitotic spindle formation in vertebrates. *Curr. Biol.* **10**, 59-67.

Lydersen, B. K. and Pettijohn, D. E. (1980). Human specific nuclear protein that associates with the polar region of the mitotic apparatus: distribution in a human/hamster hybrid cell. *Cell* **22**, 489-499.

Maekawa, T., Leslie, R. and Kuriyama, R. (1991). Identification of a minus-end specific microtubule-associated protein located at the mitotic spindle poles in cultured mammalian cells. *Eur. J. Cell Biol.* **54**, 255-267.

McIntosh, J. R. and Koonce, M. P. (1989). The mitotic spindle. *Science* **246**, 622-628.

Merdes, A., Raymar, K., Vicchio, J. D. and Cleveland, D. W. (1996). A complex of NuMA and cytoplasmic dynein is essential for mitotic spindle assembly. *Cell* **87**, 447-458.

Merdes, A., Heald, R., Samejima, K., Earnshaw, W. C. and Cleveland, D. W. (2000). Formation of spindle poles by dynein/dynactin-dependent transport of NuMA. *J. Cell Biol.* **149**, 851-861.

Mitchison, T. J. (1989). Mitosis: basic concepts. *Curr. Opin. Cell Biol.* **1**, 67-74.

Olmsted, J. B., Stemple, D. L. Saxton, W. M., Neighbors, B. W. and McIntosh, J. R. (1989). Cell cycle-dependent changes in the dynamics of MAP2 and MAP4 in cultured cells. *J. Cell Biol.* **109**, 211-223.

Price, C. M. and Pettijohn, D. E. (1986). Redistribution of the nuclear mitotic apparatus protein (NuMA) during mitosis and nuclear assembly. *Exp. Cell Res.* **166**, 295-311.

Rieder, C. (1991). Mitosis: toward an understanding of chromosome behavior. *Curr. Opin. Cell Biol.* **3**, 59-66.

Rieder, C. L. and Cole, R. W. (1998). Perfusion chambers for high-resolution video light microscopic studies of vertebrate cell monolayers: some considerations and a design. *Methods Cell Biol.* **56**, 253-275.

Saredi, A., Howard, L. and Compton, D. A. (1996). NuMA assembles into an extensive filamentous structure when expressed in the cell cytoplasm. *J. Cell Sci.* **109**, 619-630.

Saredi, A., Howard, L. and Compton, D. A. (1997). Phosphorylation regulates the assembly of NuMA in a mammalian mitotic extract. *J. Cell Sci.* **110**, 1287-1297.

Sparks, C. A., Fey, E. G., Vidair, C. A. and Doxsey, S. J. (1995). Phosphorylation of NuMA occurs during nuclear breakdown and not mitotic spindle assembly. *J. Cell Sci.* **108**, 3389-3396.

Stenoien, D. L., Sen, S., Mancini, M. A. and Brinkley, B. R. (2003). Dynamic association of a tumor amplified kinase, Aurora A, with the centrosome and mitotic spindle. *Cell Motil. Cytoskeleton* **55**, 134-146.

Tousson, A., Zeng, C., Brinkley, B. R. and Valdivia, M. M. (1991). Centrophilin, a novel mitotic protein in the mammalian cell nucleus. *J. Cell Biol.* **112**, 427-440.

Yang, C. H., Lambie, E. J. and Snyder, M. (1992). NuMA, an unusually long coiled-coil related protein in the mammalian cell nucleus. *J. Cell Biol.* **116**, 1233-1237.

Zhai, Y., Kronebusch, P. J. and Borisy, G. G. (1995). Kinetochore microtubule dynamics and the metaphase-anaphase transition. *J. Cell Biol.* **131**, 721-734.